Monitoring active steam injection through time-lapse seismic refraction surveys

Byron Matthew Kelly and Donald C. Lawton

ABSTRACT

Steam-assisted gravity drainage is an effective recovery method employed to shallow heavy oil reserves to increase the amount of recoverable oil in place. To ensure effective recovery, seismic monitoring of an active steam flood is essential in delineating the location of stimulated reserves. Typically, large and dense 4D reflection surveys are recorded to trace the motion of the steam flood, observable in terms of time shifts and amplitude difference. However, time-lapse refraction profiles can be employed to monitor the movement of an active steam flood within a reservoir in a manner similar to that of 4D reflection profiles. Through the reciprocal traveltime analysis, refraction profiles can delineate significant time-shifts within a monitor survey due to the injection of a steam flood.

Time lapse refraction profiles have significantly lower time and monetary commitments than conventional 4D reflection profiles. Refractions from the Devonian carbonates can be recorded at large offsets, thus requiring fewer sources to survey an extensive area.

This study will outline the basis for 4D refraction surveying through simple numerical modeling of a typical shallow, heavy oil reservoir.

INTRODUCTION

Steam assisted gravity drainage (SAGD) in-situ recovery is a process applied to heavy oil reservoirs to aid in the removal of bitumen via heating through convection of injected steam. This process of injecting steam into a highly viscous reservoir elevates the temperature of bitumen to a point that allows for gravity driven drainage downward through a steam chamber into a production well. Within western Canada, SAGD processes have been adopted as the primary recovery method for producing bitumen from the shallow McMurray Formation reservoirs within the Athabasca oil-sands deposits (Bianco 2008).

Monitoring SAGD processes is an important aspect of successful recovery operations (Collins 2005). Seismic monitoring techniques are dominantly 4D reflection surveys over which steam front movements can be monitored through amplitude or travel time differences between a baseline and a monitor survey. However, time-lapse refraction profiles can be employed to monitor SAGD recovery processes in much the same respect as 4D reflection profiles. Modified from a technique developed by Hansteen et al., (2010), this study models a time-lapse refraction survey for a McMurray Formation reservoir that has undergone SAGD recovery processes, via simple numerical modeling. It is proposed that time-lapse refraction surveys can be an effective monitoring technique for active SAGD recovery within shallow reservoirs, with a significantly lower time and monetary commitments than conventional reflection surveys (Hansteen et al., 2010).

SURVEY DESIGN

The refraction survey modelled consists of a single refraction line containing two reciprocal shot points located 335 m from the first geophone, which is equivalent to the crossover distance to detect first refracted arrival from the Devonian carbonates underlying the McMurray formation reservoirs at a depth of 80 m. The center of the array consists of 20 single component geophones with 20 m separation. Each shot point location also has one single component geophone (Figure 1). To provide sufficient areal coverage refraction lines are recorded in a radial pattern, every 11 degrees, to simulate a large, dense pad of geophones (Figure 20).

The refraction survey is employed pre and post steam injection, to record a baseline and four monitor surveys to model different steam chamber growth. Travel time differences due to steam injection are observed as time-shifts recorded on first arrival head waves. By placing a geophone at the shot point locations, ambiguity is removed from observed time-shifts by subtracting travel times on the source side of the array, leaving only time-shifts due to steam injection within the reservoir. The location of steam injection will be midway between the two source locations. Figure 1, shows a schematic model and survey design, and projected ray paths for refractions from the underlying Devonian carbonate.

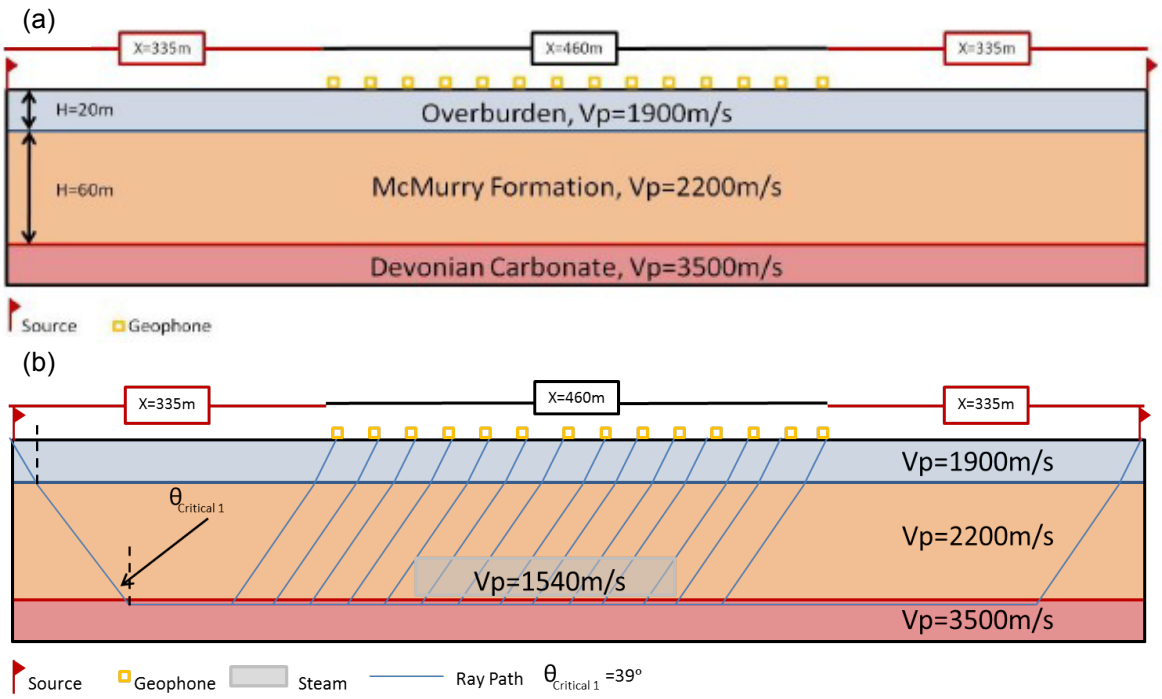

Figure 1. (a) Geological model and survey design. Note that each source location also contains one single component geophone. (b) Projected ray path from shot point A to B (forward) refracting along the carbonate layer. Note that rays traveling upward through the steam zone will have a different Θ critical than those traveling in the non-heated McMurray Formation.

MODEL DESIGN

Time-lapse refraction surveys were numerically modeled over a schematic reservoir undergoing active SAGD recovery. For simplicity, surveys were modeled over layer-cake geometry with average formation thickness and depth appropriate for a shallow oil sands deposit (Figure 1a). All formations overlying the McMurray formation are referred to as overburden, with a thickness of 20m and an average P-wave velocity of 1900m/s. All model parameters are outlined in Table 1 (Lines et al., 1990; Bianco, 2008; Eastwood, 1993; Forgues et al., 2006). Dimensions of the simulated steam chamber are listed in Table 2.

Other simplifications have been applied to the model. We assume that the McMurray Formation sands are homogeneous, containing negligible amounts of shaly sand and free of flow barriers which would restrict homogeneous steam chamber growth (Chen, 2009). Second, we are basing this model on only P-wave velocity changes, hence ignoring density. Third, we are not including a low velocity weathering layer in our model, thus ignoring any near surface effects. Lastly, this model will not take into account issues with repeatability, noise contamination or signal-to-noise ratio. Although these simplifications do not represent real world situations, this model serves to lay the foundation for SAGD time-lapse refraction monitoring, modified from the approach of Hansteen et al., (2010).

Formation	Thickness	P-wave Velocity	Heated Velocity
Overburden	20 meters	1900 m/s	N/A
McMurray	60 m	2200 m/s	1540 m/s
Devonian Carbonates	N/A	3500 m/s	N/A

Table 1. Model Parameters

Model Number	Height	Length of Steam Chamber
1	60	140 m
2	60	80 m
3	30	140 m
4	30	80 m

Table 2. Model dimensions and parameters

Changes in velocity values due to steam injection are largely dependent on temperature, when temperatures exceed 60^{o}C, and where higher bitumen saturation will lead to higher velocity sensitivity (Chen, 2009; Eastwood, 1993; Lines et al., 1990; Wang et al., 1988). For high saturation values, P-wave velocity can serve as a potentially accurate thermometer. For example, at 100% bitumen saturation and temperatures of 100-250 ^{o}C,

P-wave velocity decreases by an average of 40% (Tosaya et al., 1987). For this study, we model bitumen saturation values of 80%, providing a P-wave velocity decrease of 30% (2200 m/s to 1540 m/s) (Chen, 2009; Bianco, 2008; Eastwood, 1993). The bounds of the steam chamber will include a linear velocity taper to simulate the progressive reduction of heat as we move away from the limits of the steam chamber.

Initial modeling results for the baseline survey were compared with synthetics develop using SeisImager software to confirm the accuracy of modeled travel times within the unheated reservoir. This comparison yielded a high degree of correlation, supporting the accuracy of the baseline survey traveltime calculations (Figure 2).

DATA INTERPRETATION AND RESULTS

Traveltime curves produced from the four different models were interpreted using the plus-minus method to check for consistency in observed layer depths and velocity values. Calculated values form the traveltime graphs showed a high degree of consistency with input values, confirming the plus-minus technique as a valid analysis method for this three layer system.

To quantify the changes due to simulated steam injection, traveltime values from the baseline survey were subtracted from values in each monitor survey, leaving only time-shifts within the reservoir. However, this simplistic approach requires further consideration. Traveltime changes observed on a monitor survey may be caused by time differences on the source side rather than the presence of a steam chamber on the receiver leg of a refraction raypath. For instance, changes on the source side of the array, potentially introduced through issues such as changes in source statics, may introduce slight time shifts which may be wrongfully attributed to changes within the reservoir. To mitigate this, we calculated and removed the traveltimes of the downgoing transmitted wave field from the source point, leaving only traveltimes for the headwaves refracting along the Devonian carbonates and propagating upward through the reservoir (Figure 4). Removing this component of the traveltime plot has decreased the likelihood that traveltimes changes are due to sources other than steam injection within the reservoir. These travel times can be quantified through a calculation of the T^+ component, where $T^+ = T_{AD} + T_{HD} - T_{AH}$ (Figure 5). In a time-lapse sense, we are comparing differences in T^+ traveltimes.

Hence, we can effectively determine the traveltime for the downgoing portion of the wavefield for each monitor survey, resulting in time differences attributable only to the upgoing wavefield through the steam zone. Figures 7-9 are traveltime charts for model 1, displaying the steam induced time-shifts after subtraction of the downgoing wavefield traveltime. Figures 13-15 are traveltime charts for model 3, a steam chamber occupying half the thickness of the McMurray formation. Time-shift values between models 1 and 3 vary considerably due to the difference in the thickness of the steam chamber.

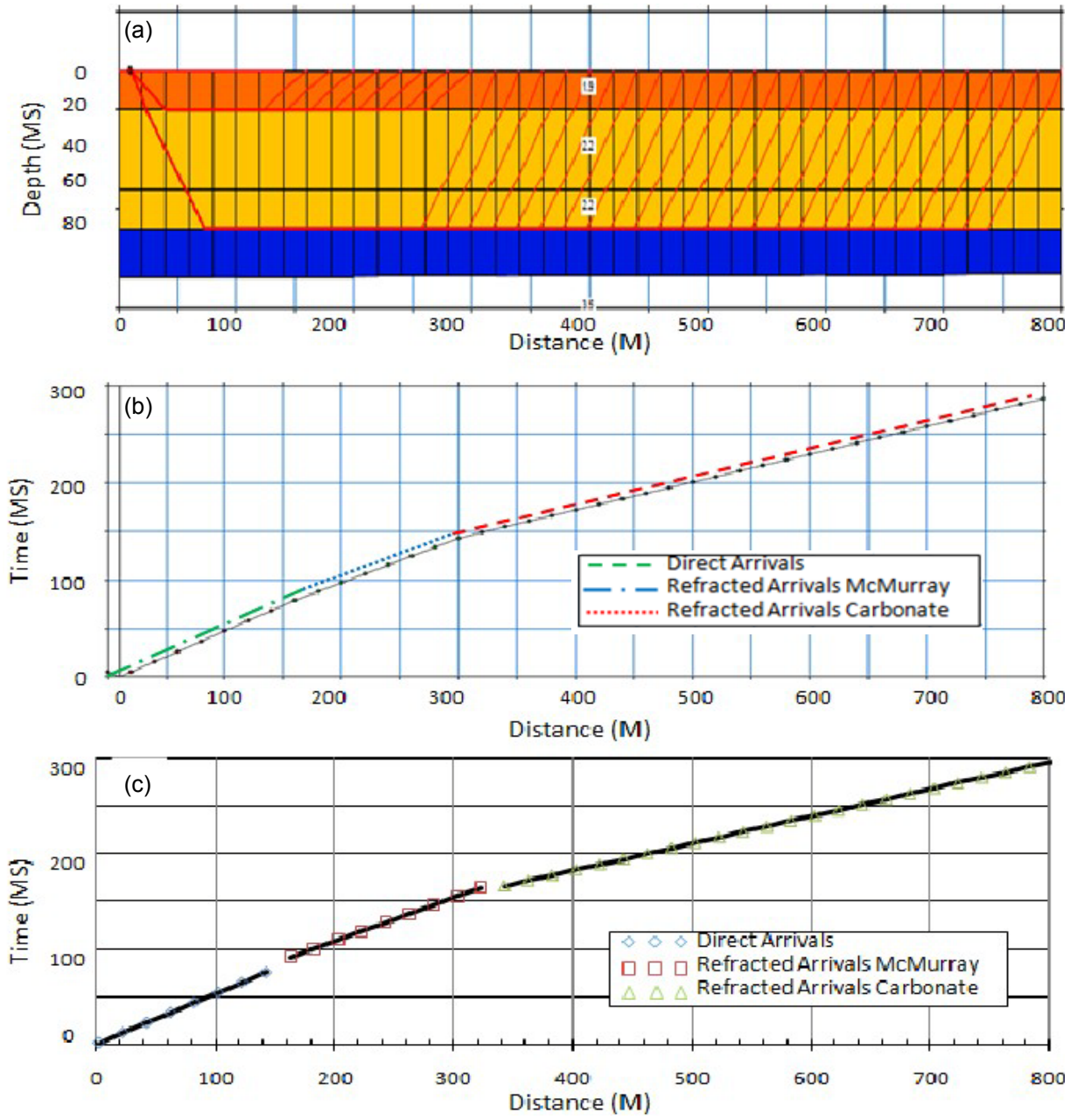

Figure 2. (a) Baseline model produced with SeisImager. Red lines indicate raypaths. (b) Synthetic traveltime plot produced with SeisImager. (c) Synthetic traveltime plot produced from calculations. Note that both traveltime plots produce very similar results.

From observing these traveltime charts, it is important to note two things. Firstly, time-shifts of model 3 and not half that of model 1, despite the steam chamber being half the size in model 3 than in model 1. This shows a non-linear relationship between steam chamber thickness and observed time-shifts. Secondly, surface locations of steam chamber time-shifts are not the same as subsurface locations of the steam chamber, due to the path that refracted rays travel when returning back to the surface. Thus, a ray tracing is required to backproject observed time-shifts to their subsurface location. This

redatuming of the wavefield will enhance the spatial resolution of the observed time shifts (Hansteen et al., 2010).

Comparing models 1&3 to models 2&4, similar conclusions can be drawn regarding the time-shift differences between the two steam chamber thicknesses. The only difference lies in the number of receivers which detect time-shifts, due to the decrease in the lateral extent of the steam chamber. Model 4, which has the smallest steam chamber (30m X 80m), the time-shifts are the most subtle and may be more difficult to detect within real data than a large steam chamber, such as Model 1. Nevertheless, time shifts for the two steam chamber thickness (15ms and 5ms) are larger than the calculated error of +/- 1 ms and hence detectable within modeled data.

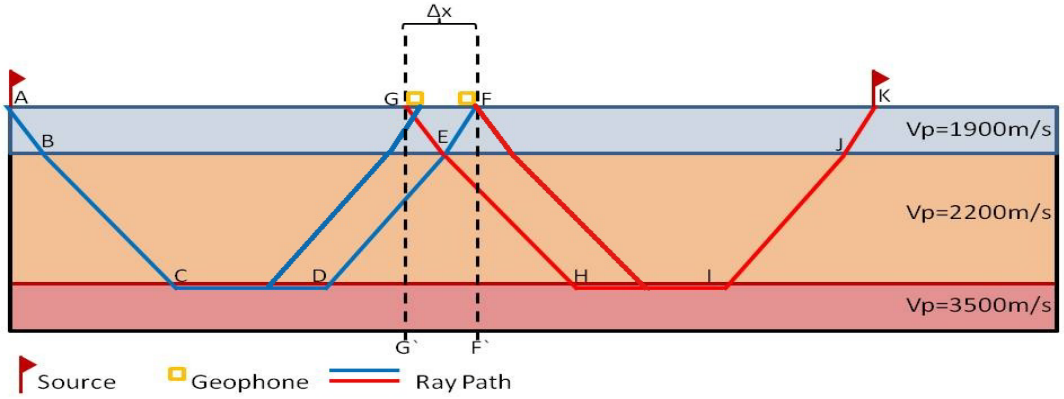

Figure 4. Travel time paths used in the plus-minus calculation for T^{-}.

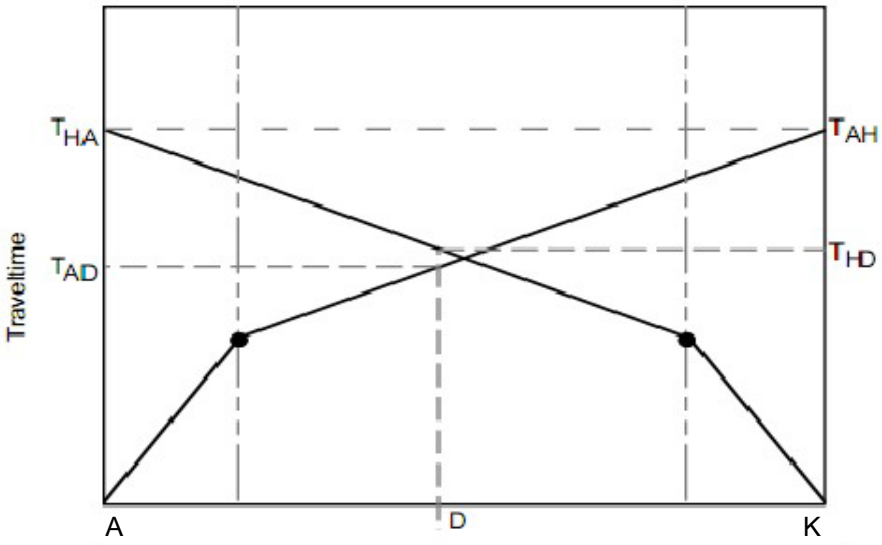

Figure 5. Schematic time travel chart used for the plus-minus calculations. D = midpoint (Chen, 2009).

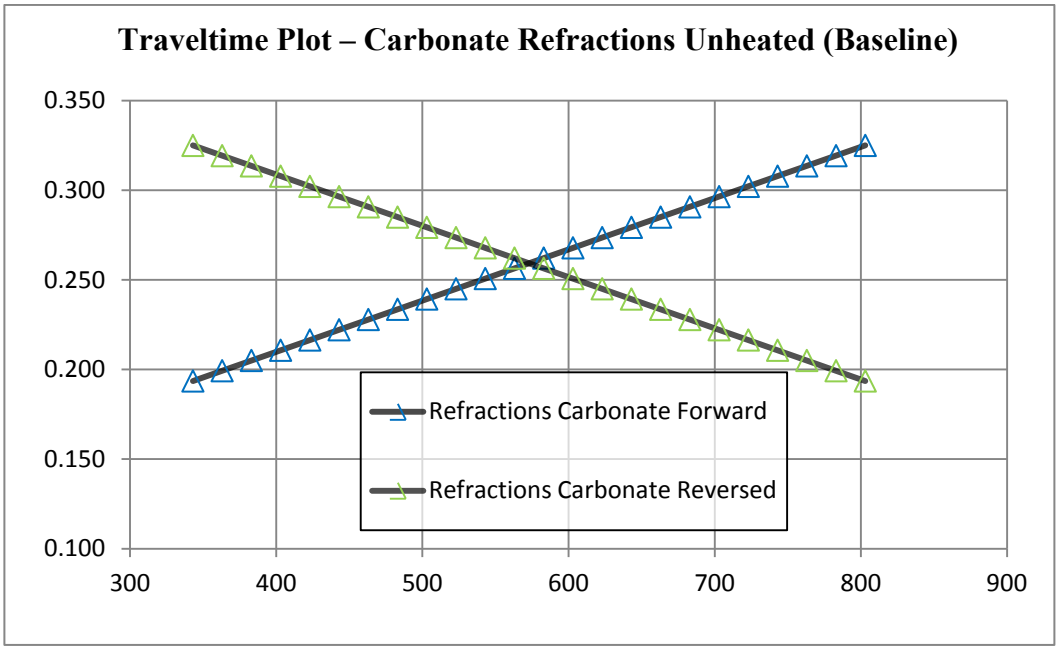

Figure 6. Traveltime plot for model 1 displaying refracted arrivals from the Devonian carbonate after the subtraction of the traveltime for the downgoing wavefield.

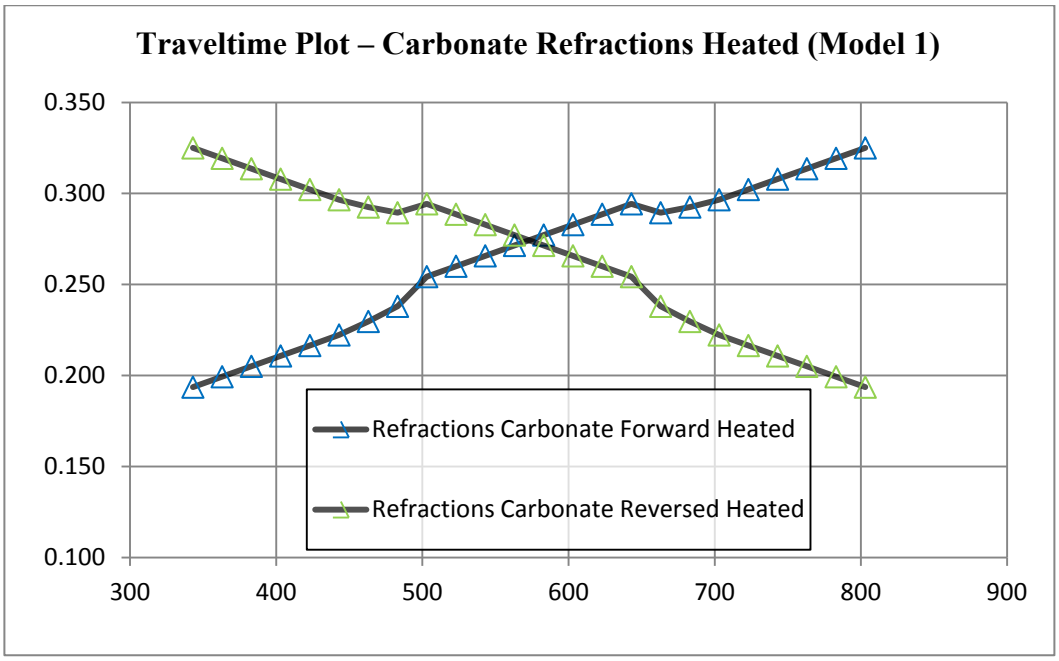

Figure 7. Traveltime plot for model 1 after the addition of a 140m steam chamber. Time-shifts are observable on both the forward and reverse profiles.

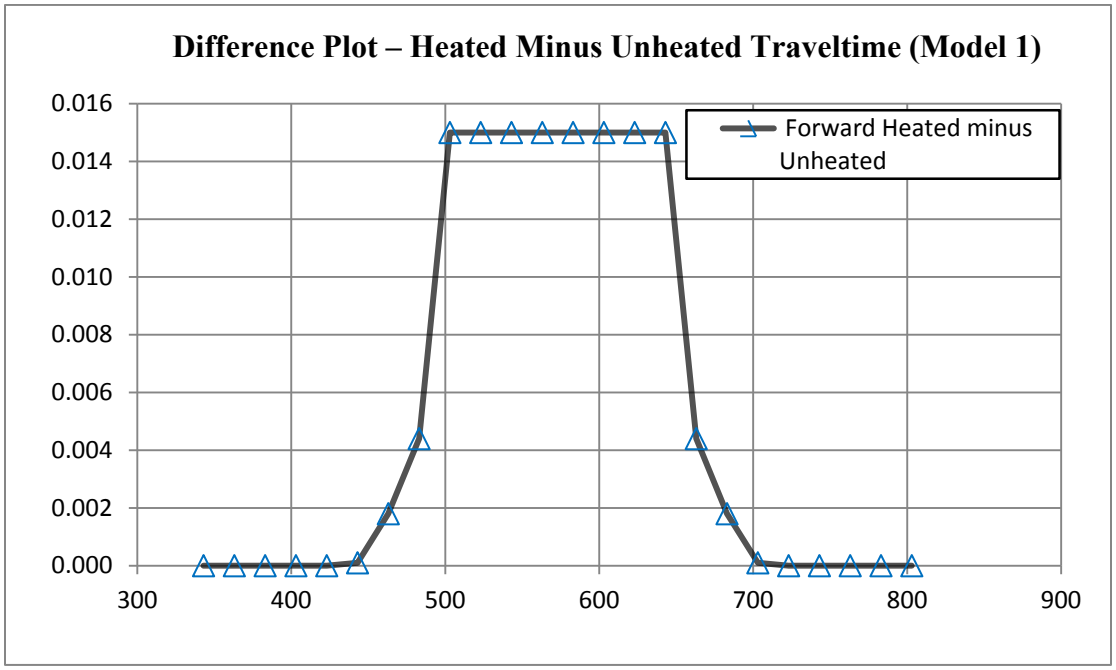

Figure 8. Difference plot of the forward refraction profile of model 1, showing the traveltime difference between the unheated and heated reservoir.

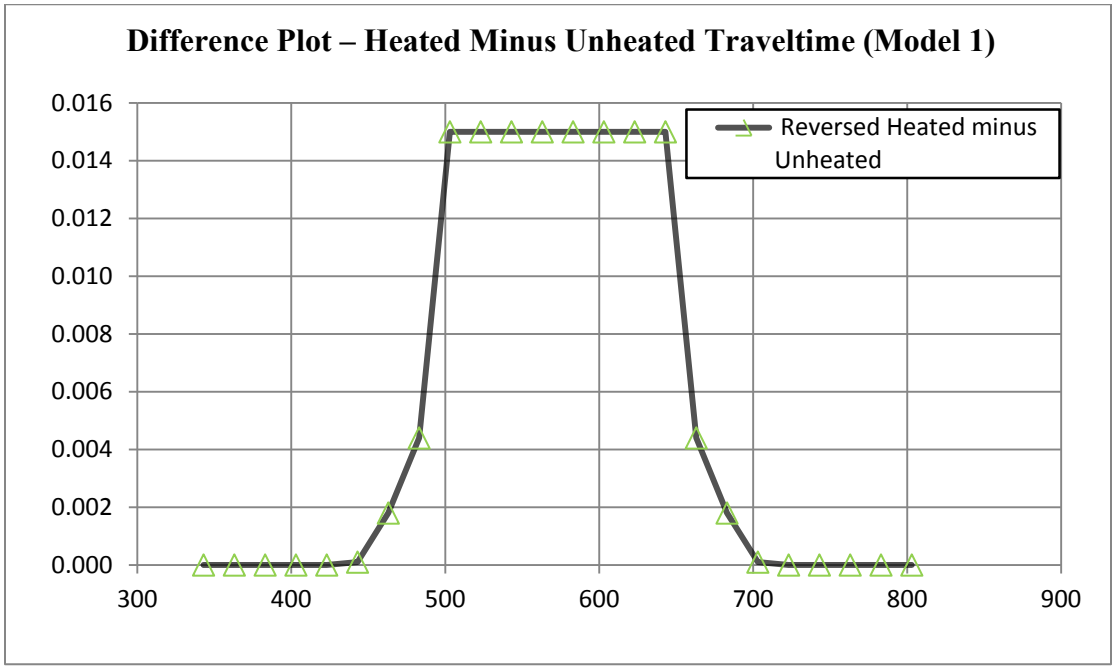

Figure 9. Difference plot of the reverse refraction profile of model 1, showing the traveltime difference between the unheated and heated reservoir.

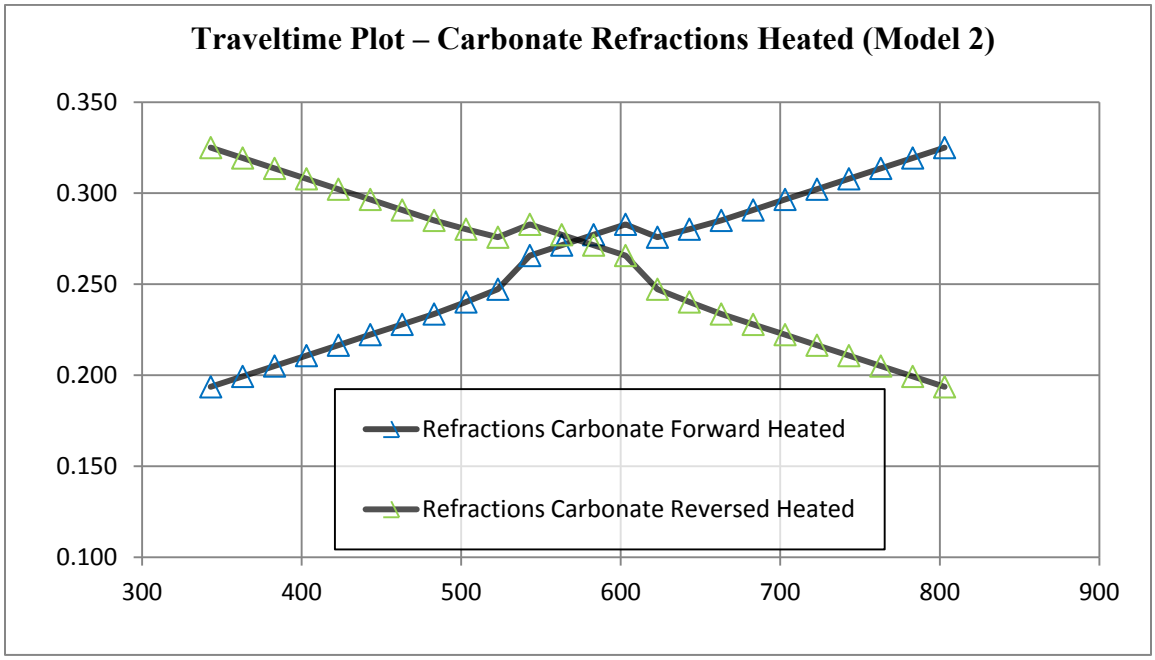

Figure 10. Traveltime plot for model 2 with a 80m steam chamber. Time-shifts are observable on both the forward and reverse profiles.

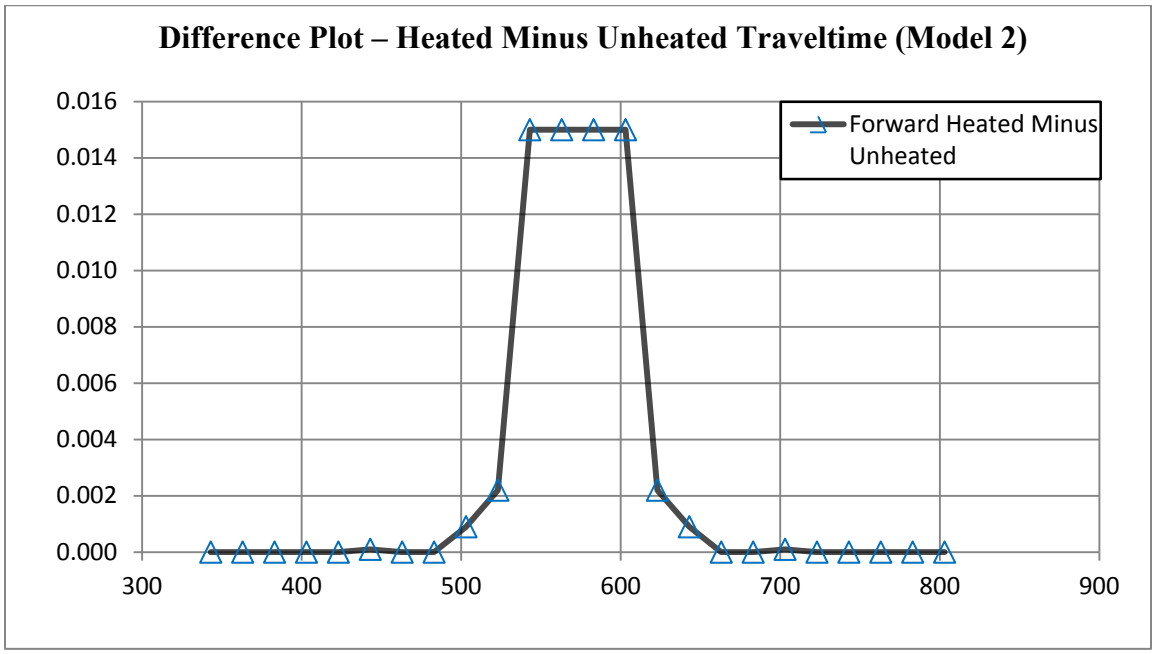

Figure 11. Difference plot of the forward refraction profile of model 2, showing the traveltime difference between the unheated and heated reservoir.

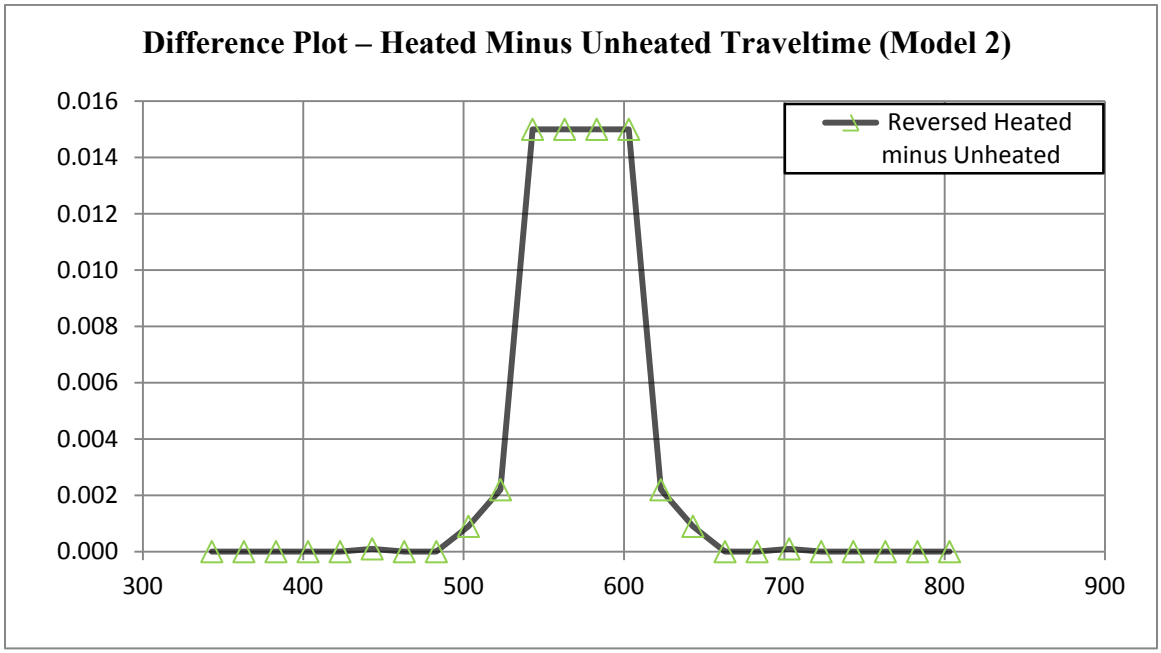

Figure 12. Difference plot of the reverse refraction profile of model 2, showing the traveltime difference between the unheated and heated reservoir.

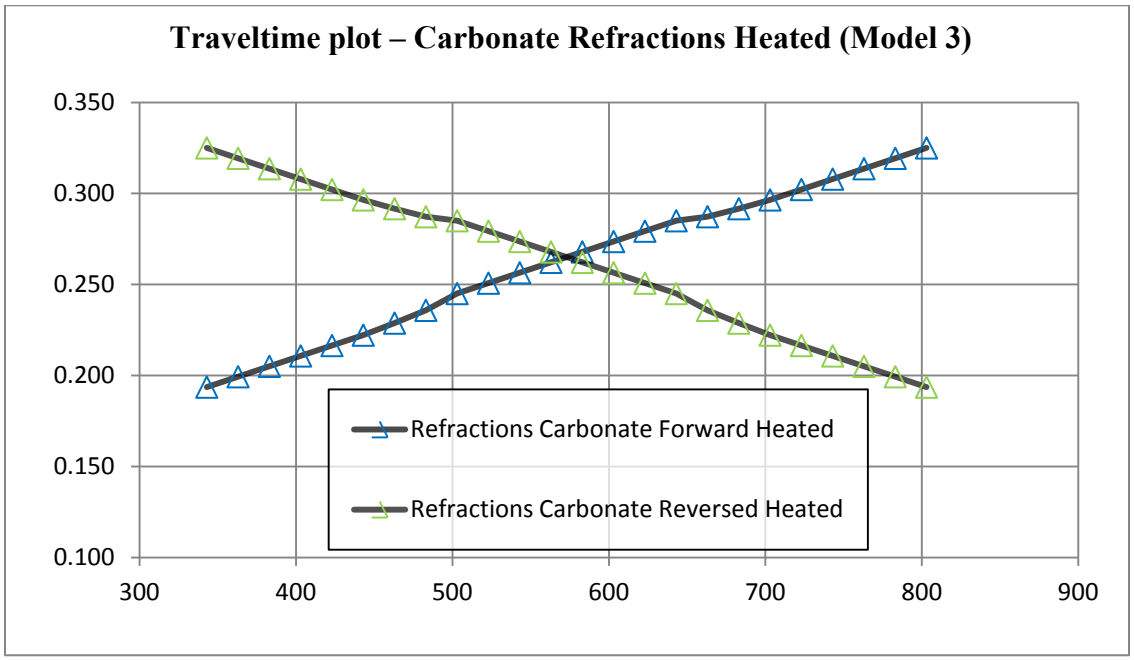

Figure 13. Traveltime plot for a steam chamber 140m and 30m thick. Time-shifts are more subtle than for models 1, 2, but still observable.

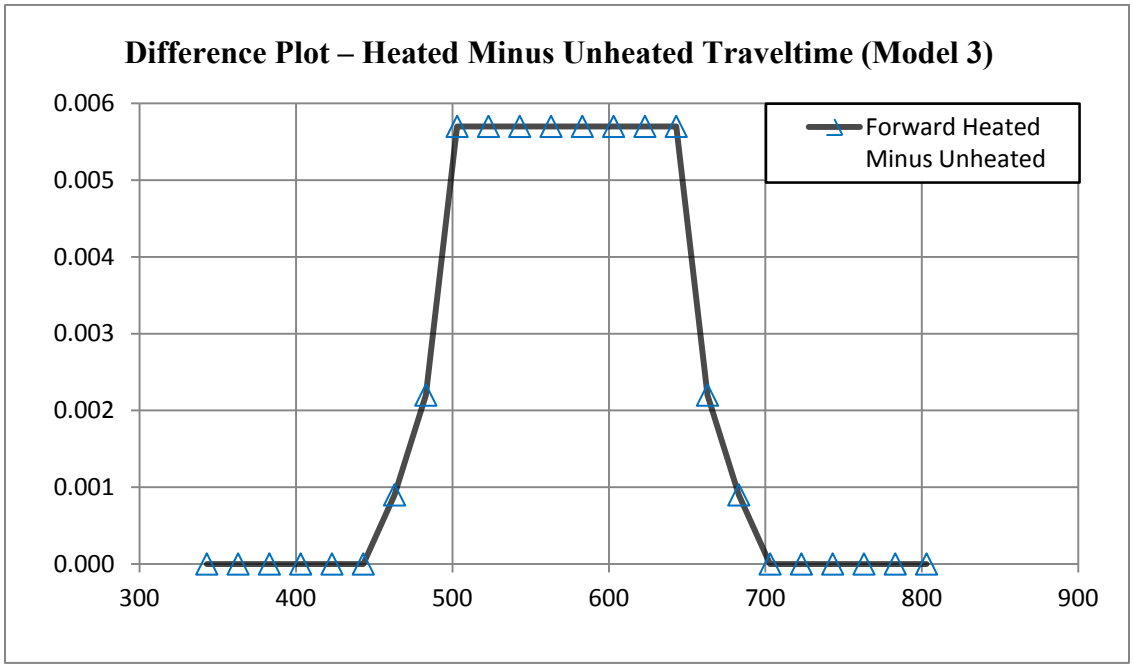

Figure 14. Difference plot of the forward refraction profile of model 3, showing the traveltime difference between the unheated and heated reservoir. Traveltime differences are smaller than those observed within the thicker steam chamber.

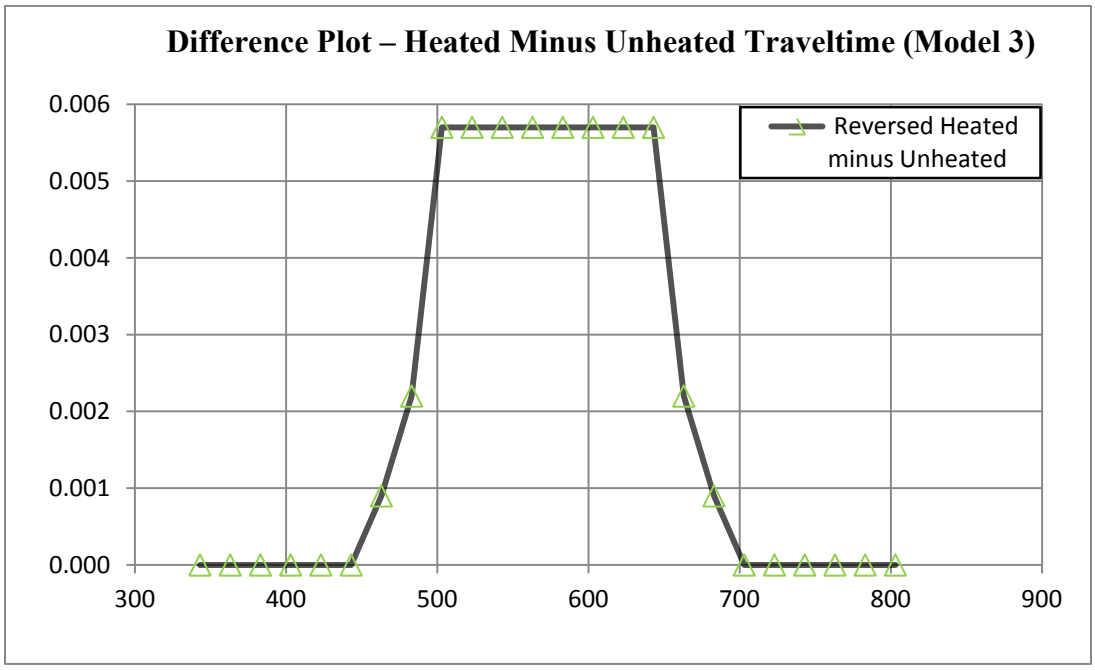

Figure 15. Difference plot of the reverse refraction profile of model 3, showing the traveltime difference between the unheated and heated reservoir. Traveltime differences are smaller than those observed within the thicker steam chamber.

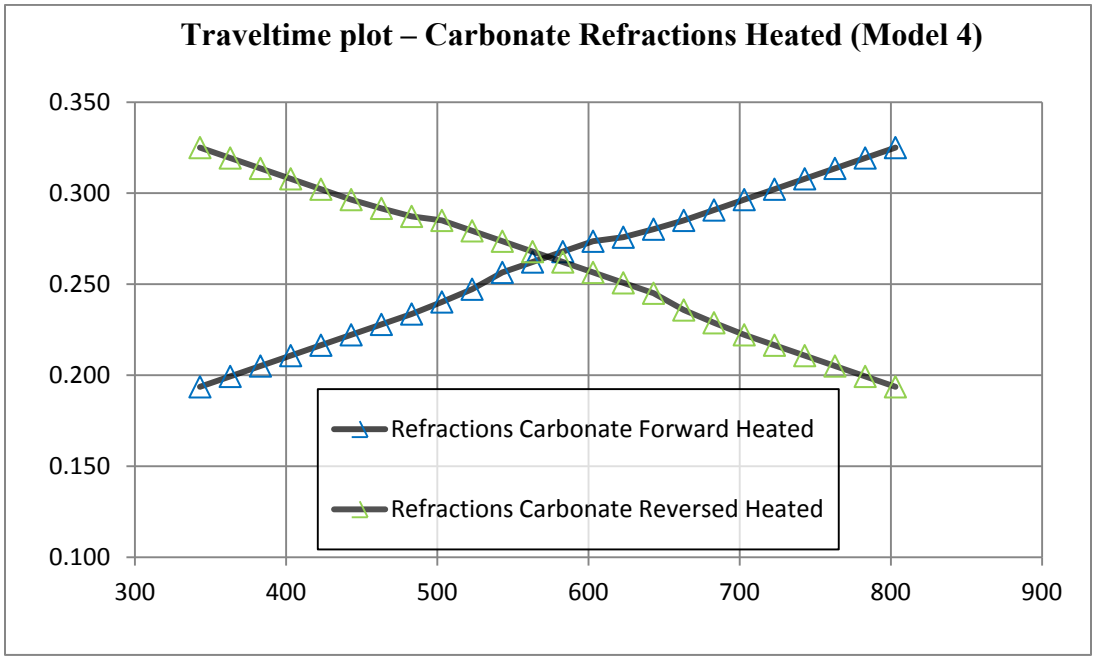

Figure 16. Traveltime plot for a steam chamber 8m wide and 30m high. Time-shifts are the most subtle of all modeled steam chambers, but still observable.

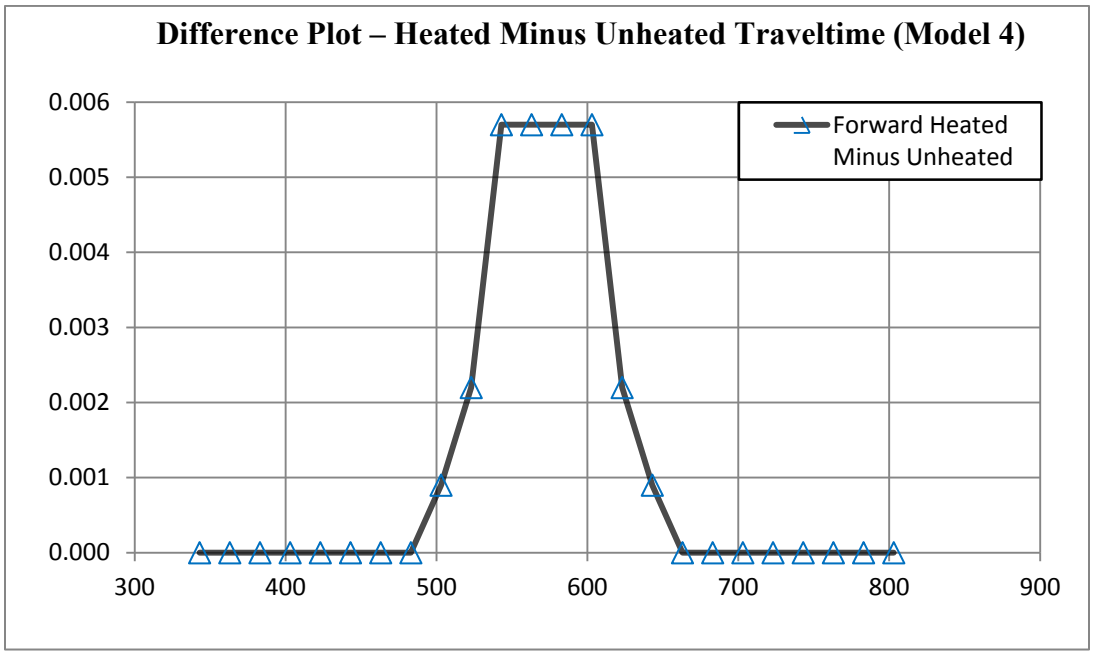

Figure 17. Difference plot of the forward refraction profile of model 4, showing the traveltime difference between the unheated and heated reservoir. Traveltime differences are smaller than those observed within the thicker steam chamber, and extend over a smaller area due to the reduction in steam chamber length.

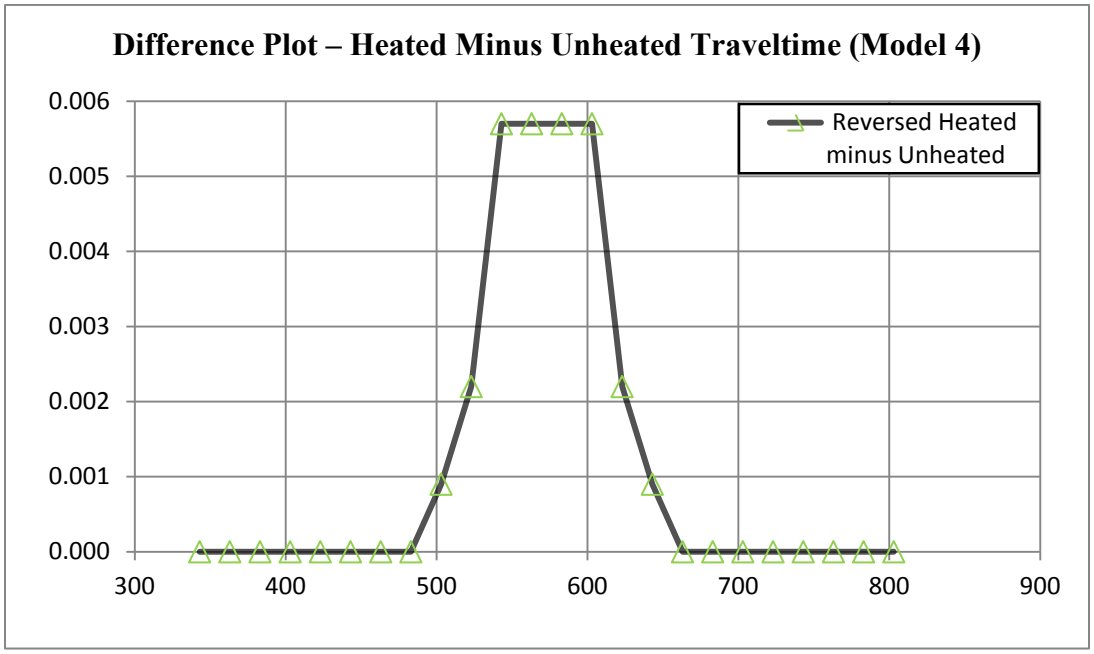

Figure 18. Difference plot of the reverse refraction profile of model 4, showing the traveltime difference between the unheated and heated reservoir. Traveltime differences are smaller than those observed within the thicker steam chamber, and extend over a smaller area due to the reduction in steam chamber length

Observed traveltime changes along a modeled 2D refraction line were projected into 3D in an azimuthal distribution and plotted in map view (Figure 20). Due to the symmetry of the model and the applied velocity taper, observed time-shifts form a bull's-eye pattern, showing the extent of the steam chamber, as well as the reduction in heat (increase in velocity) with increasing distance from the injection location. Figure 21 represents the azimuthal survey design, and Figures 21-24 display observed time-shifts for models 1-4.

Models 1 and 2 have the same time-shift values, but due to the difference in steam chambers dimensions, model 1 extends over a large area than model 2. Models 3 and 4 have a lower time-shift value than models 1 and 2 due to the steam chamber occupying half the thickness of the McMurray formation than in models 1 and 2.

REAL DATA POTENTIAL

The image shown in figure 19 is from a 4D heavy oil dataset from Northern Alberta. This data has not been processed, and has only AGC applied to enhance the visibility of reflections and refractions. The Devonian carbonate is located at ~222m depth, and thus would require offsets of >700m to detect refracted arrivals from the Devonian interface.

As illustrated in figure 19, we have strong reflections from the Devonian carbonate at 300ms as well as Devonian refractions as first arrivals on the far offsets. This record, however, has limited offset (max offset ~800m) and thus only detects a small segment of the Devonian refraction as first arrival energy. With greater offsets we would see sufficient refractions from the carbonate surface to apply time-lapse refraction analysis.

Hence, this data example supports the idea that we can detect Devonian refractions on conventional reflection data (as well as refraction data) to which we could apply our time-lapse refraction analysis.

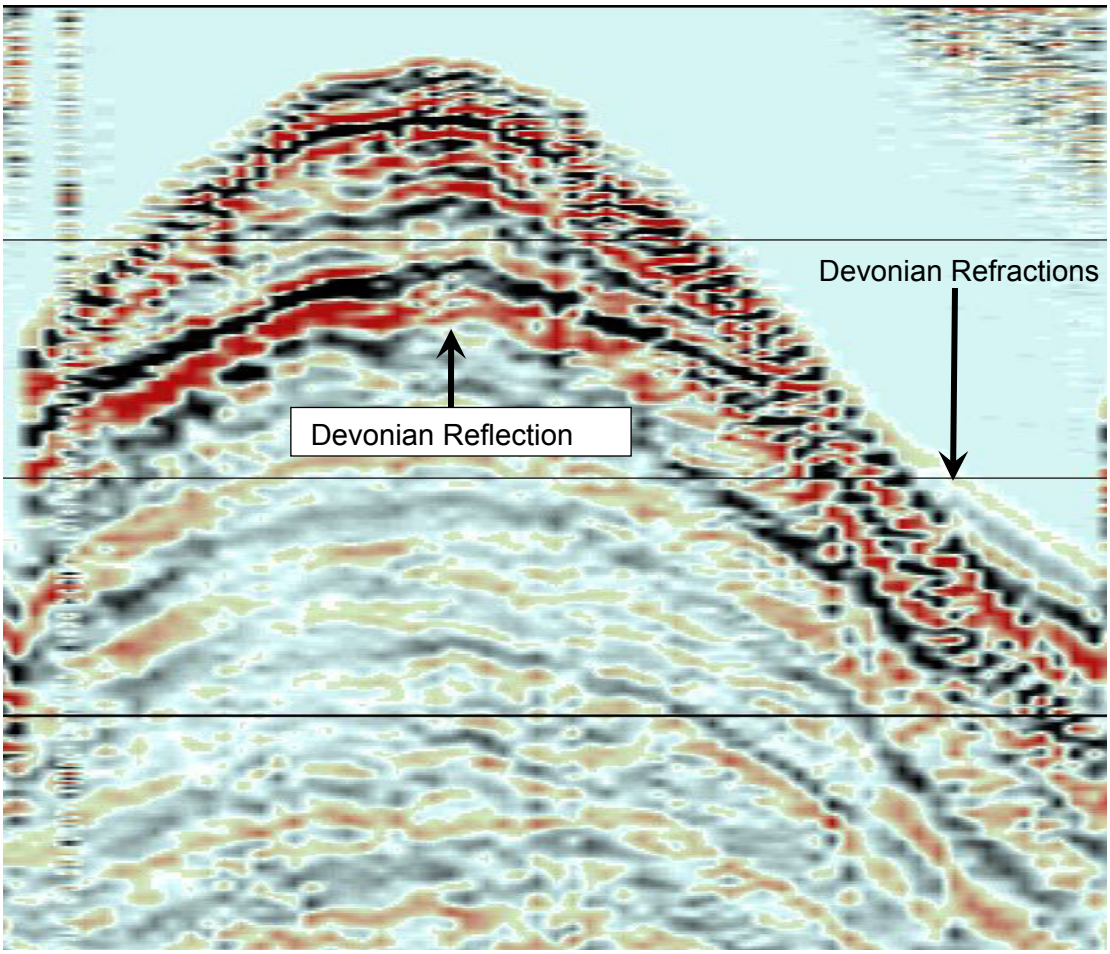

Figure 19. Raw data from a heavy oil area, Northern Alberta. Devonian reflections and refractions are annotated. Max offset = ~800m.

CONCLUSIONS

SAGD is an effective recovery method employed to shallow heavy oil reserves to increase the amount of recoverable oil in place. However, to ensure effective recovery, seismic monitoring of an active steam front is essential in delineating the location of stimulated reserves. Time-lapse refraction profiles can be employed to monitor the movement of an active steam front within a reservoir similar to that of 4D reflection profiles. Also, because refractions from the Devonian carbonate can be viewed at large offsets from the source locations, the survey extent of a single source is significantly greater than that of reflection profiles, thus requiring fewer sources to monitor extensive areas, reducing surveying costs (Hansteen et al., 2010).

This technique has been previously developed by Hansteen et al., in 2010, but has been modified by removing the traveltime of the downgoing wavefield on the source side of the array, effectively reducing the uncertainty associated with observed time-shifts.

Error values of the calculated plus and minus traveltimes are in the range of +/- 1.0 ms, a considerable amount less than observed time-shifts from steam injection.

Following our observations, we propose that time-lapse refraction surveys can be an effective monitoring technique for active SAGD recovery within shallow reservoirs, with potentially significantly lower time and cost commitments than conventional 4D reflection profiles. However, this modeling study outlines only the basis for effective 4D refraction surveying. Further considerations are required to further our understanding of this technique. Assumptions and simplifications employed, such as homogeneity, isotropy, repeatability, signal to noise ratio and noise contamination must be address in further studies to support the development of 4D refraction surveys over active SAGD reservoirs.

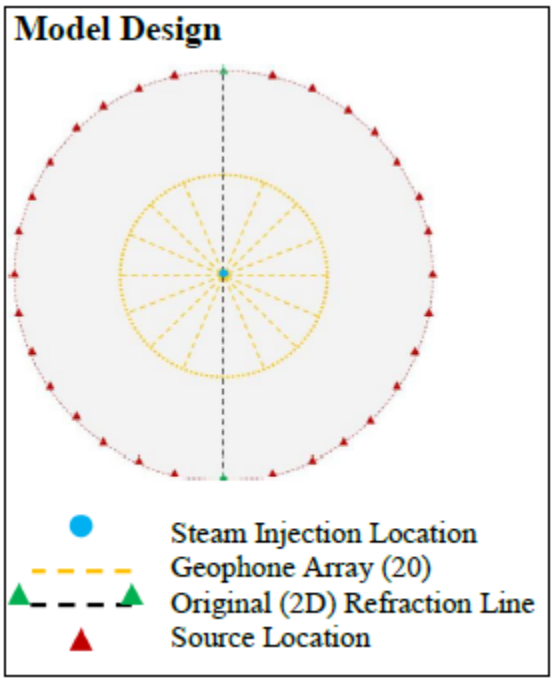

Figure 20. 3D survey design. Refraction lines are projected in an azimuthal distribution every 11 degrees. Geophone array in the center overlies the expected steam chamber location, acting as a single large pad of densely spaced receivers.

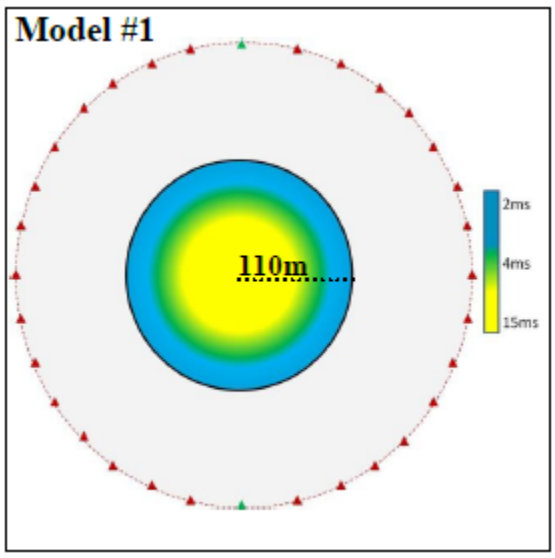

Figure 21. Model 1. Time-shifts due to heating a steam chamber with a 80m radius, 60m thick and 30m velocity taper, simulating a large steam chamber heating the entire thickens of the McMurray Formation. Decreases in time-shifts towards the edges of the steam chamber are due to gradual decrease in heating.

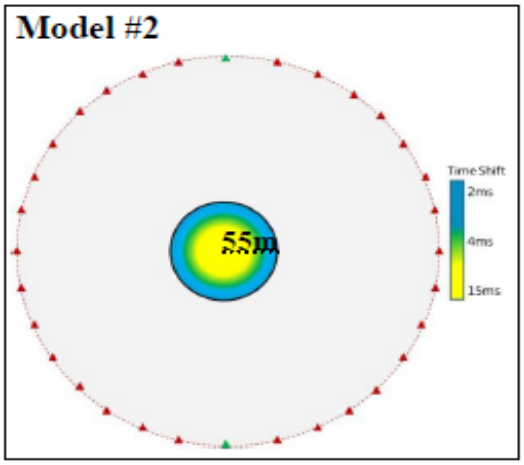

Figure 22. Model 2. Time-shifts due to heating a steam chamber with a 40m radius, 60m thick, and 15m velocity taper, simulating a smaller steam chamber heating the entire thickness of the McMurray Formation. Decreases in time-shifts towards the edges of the steam chamber are due to gradual decreases in heat. Note that time-shift values are the same as in Model 1, but with a smaller radial distribution.

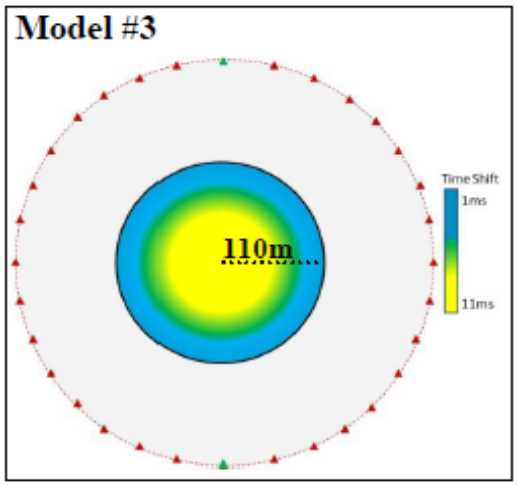

Figure 23. Model 3. Time-shifts due to heating a steam chamber with a 80m radius, 30m thick, and 30m velocity taper, simulating a larger steam chamber heating the lower half of the McMurray Formation. Decreases in time-shifts towards the edge of the steam chamber are due to gradual decreases in heating. Time-shift values are lower than in model 1 due to smaller steam chamber size.

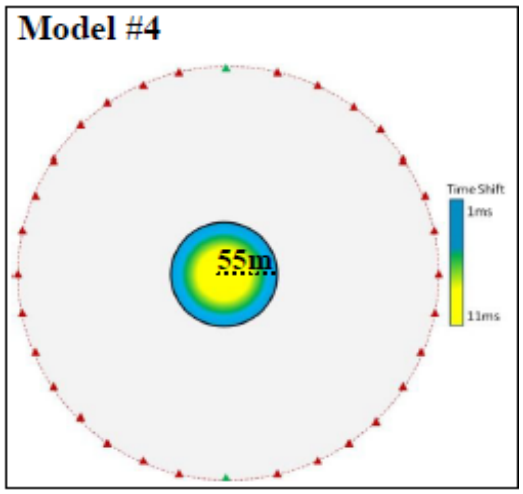

Figure 24. Model 4. Time-shifts due to heating a steam chamber with a 40m radius, 30m thick, and 15m velocity taper, simulating a steam chamber heating the lower half of the McMurray Formation. Decreases in time-shifts towards the edges of the steam chamber are due to gradual decreases in heat. Time-shift values are lower than in model 2 due to the smaller steam chamber size.

ACKNOWLEDGMENTS

We would like to thank CREWES and the CREWES sponsors for supporting this research.

REFERENCES

Bellman, L.W., 2007, Oil sands reservoir characterization. A case study at Nexen/Opti Long Lake: 2007 CSPG CSEG Convention, 640-641.

Bellows, L., Bohme, V., 1963, Athabasca oil sands: Journal of Petroleum Technology, v.15, No.5, 479-783.

Bianco, V., Kaplan, S., Schmitt, D., 2008, Seismic rock physics of steam injection in bituminous oil reservoirs: The Leading Edge, 11332-1137.

Chen, Q., 2009, Assessing and improving steam assisted gravity drainage: Reservoir heterogeneities, hydraulic fractures and mobility control foams: PHD Thesis, Stanford University.

Collins, P.M., 2005, Geomechanical effects on the SAGD process: SPE/PS-CIM/CHOA International Thermal Operations and Heavy Oil Symposium, 1-11.

Dufour, J., Foltinek, D.S, 1996, The plus-minus time analysis method and itsimplementations: CREWES Research Reports vol.8, 13-1 - 13-33.

Eastwood, J., 1993, Temperature-dependant propagation of P- and S-waves in cold Lake oil sands: Comparison of theory and experiment: Geophysics, vol.58, No.6, 863-872.

Forgues, E., Meunier, J., Gresillon, F.X., Hubans, C., 2006, Continuous high-resolution seismic monitoring of SAGD, SEG/New Orleans Annual Meeting, 3165-3169.

Hansteen, F., Wills, P., Homman, K., Jin, L., 2010, Time-lapse refraction seismic monitoring: SEG Denver Annual Meeting, 4170-4174.

Hein, F.J., Cotterill, D.K., Berhane, H., 2007, an atlas of lithofacies of the McMurray Formation Athabasca Oil Sands deposits, Northeastern Alberta: Surface and subsurface: Earth Sciences Report, Alberta Energy and Utilities Board, Alberta Geological Survey.

Lines, L., Jackson, R., Covey, J., 1990, Seismic velocity models for heat zones in Athabasca Tar Sands: Geophysics, vol.55, No.8, 1108-1111.

Mossop, G.D.,1980. Geology of the Athabasca Oil Sands: Science, vol.207, 145-152.

Tosaya, C., Nur, A., Dung, V., Da Prat, G., 1987, Labratory seismic methods for remote monitoring of thermal EOR: SPE Reservoir Engiineering, 235-242.

Wang, Z., Nur, A., 1988, Effect of temperature on wave velocities in sands and sandstones with heavy hydrocarbons: Borehole Geophysics 1, 3-5.